Available online at www.sciencedirect.com
SCIENCE DIRECT®
ELSEVIER
International Journal of Multiphase Flow 31 (2005) 593–617
International Journal of Multiphase Flow
www.elsevier.com/locate/ijmulflow

Methodological improvement of an intrusive four-sensor probe for the multi-dimensional two-phase flow measurement

Xiuzhong Shen [a], Yasushi Saito [a], Kaichiro Mishima [a,*], Hideo Nakamura [b]

[a] *Research Reactor Institute, Kyoto University, Kumatori-cho, Sennan-gun, Osaka 590-0494, Japan*
[b] *Tokai Establishment, Japan Atomic Energy Research Institute, Tokai-mura, Naka-gun, Ibaraki 319-1195, Japan*

Received 11 June 2004; received in revised form 1 February 2005

Abstract

This paper aimed to improve the four-sensor probe methodology for the multi-dimensional two-phase flow measurement. We theoretically derived the interfacial measurement theorem relating the local instantaneous interfacial velocity to local measurable velocities of the multi-sensor probe in the improvement. Based on this theorem, theoretical measurement methods for the local instantaneous interfacial normal direction and the local time-averaged interfacial area concentration (IAC) using the four-sensor probe were presented. An interface-pairing signal-processing scheme was proposed to identify the same interfaces from the sequential signals detected by different sensors. The practical application of the improved IAC methodology to the two-phase flow in a vertical large diameter pipe showed that the four-sensor probes (together with the interface-pairing signal-processing scheme) could effectively measure the local time-averaged IACs with high effective interface percentages not only in the one-dimensional two-phase flow but also in the multi-dimensional two-phase flow. The measurement error analysis indicated that the errors from the bubble deformation and velocity variation due to the sensor piecing were negligible if we only applied the multi-sensor probe to the two-phase flow with the bubbles having much larger size than the sensor diameter. The total error from both the escaped and missing bubbles in the void fraction and IAC measurements was estimated at about 15.75% in the two-phase flow in a pool.

* Corresponding author. Tel.: +81 724 51 2449; fax: +81 724 51 2637.
E-mail address: mishima@rri.kyoto-u.ac.jp (K. Mishima).

0301-9322/$ - see front matter © 2005 Elsevier Ltd. All rights reserved.
doi:10.1016/j.ijmultiphaseflow.2005.02.003

Keywords: Interfacial measurement theorem; Interfacial normal direction; Interfacial area concentration; Four-sensor probe; Two-phase flow measurement

1. Introduction

One of the most characteristic features of two-phase flow is the existence of a multi-dimensionally moving interface between two phases that make theoretical predictions of flow parameters immensely more difficult than in single-phase flow. Thus, experimental measurements play a key role in providing information for design, and supporting analyses of system behavior. Since there is no effective ways for the multi-dimensional two-phase flow measurement up to now, it is very important to develop a method to measure the characteristics of the multi-dimensional two-phase flow.

Delhaye and Bricard (1994) pointed out that the geometric structure of a bubbly two-phase flow can be characterized by two of the three following parameters: the interfacial area concentration (IAC), the void fraction and the Sauter mean diameter. The IAC (a) is defined by the total interfacial area per unit mixture volume. According to Ishii (Ishii, 1975), the local time-averaged IAC at a fixed position in space $\mathbf{x}_0$ is given by

$$\bar{a}^t = \frac{1}{\Omega}\sum_l \frac{1}{|\mathbf{V}_{il}\cdot\mathbf{n}_{il}|}, \tag{1}$$

where Ω, l, $\mathbf{V}_{il}$ and $\mathbf{n}_{il}$ denote the time interval for averaging, the lth interface, the velocity vector of the lth interface, the surface normal unit vector of the lth interface at $\mathbf{x}_0$ when it passes through $\mathbf{x}_0$, respectively. The void fraction (α) is defined by the total gas phase volume per unit mixture volume. The Sauter mean diameter (d_{SM}) is given by the ratio of the volume and surface area of a typical bubble. There exists a classical expression for the three parameters, given by

$$\mathrm{d_{SM}} = \frac{6\alpha}{a}. \tag{2}$$

The intrusive multi-sensor resistance or optical probe methods for both the IAC and the void fraction measurements have been studied extensively in the past few decades. But the IAC measurement was developed from the void fraction measurement by taking advantage of the phase change signals and was much more complicated in methodology than the void fraction measurement. The basic principle for the IAC measurement with a multi-sensor probe was originally proposed by Kataoka et al. (1986). Numerous researchers showed their efforts to improve this original method in various ways. All of these IAC measurement studies using multi-sensor probes can be classified into two types, the double-sensor probe method (Kataoka et al., 1986; Hibiki et al., 1998; Wu and Ishii, 1999) and the four-sensor probe method (Kataoka et al., 1986; Revankar and Ishii, 1993; Kim et al., 2001; Euh et al., 2001). The former double-sensor probe method adopted several assumptions for bubble shape and bubble motion to enable the measurements and analyses of IAC. However, at the same time, these assumptions impose certain limitations on the application of the method. The most important and problematic assumptions are the following two ones. The first is that the bubble is spherical and the second is that the interfacial velocity can be approxi-

mated by using the ratio of two sensor tip separation and time difference when the interface passing the two sensor tips. In one-dimensional two-phase flow these assumptions may be reasonable. But in a multi-dimensional two-phase flow, due to the prevalence of the bubbly secondary flow and the heavy deformation of the bubbles, these assumptions are rather questionable. So the double-sensor probe method can only be employed in one-dimensional two-phase flow. In the later four-sensor probe method, the accurate measurements and analyses for the IAC can be achieved with no requirements for the assumption for interfacial shape and interfacial motion. But it is also only suitable for a one-dimensional two-phase flow with no or small lateral motions of the interfaces up to now because large lateral motions of the interfaces will decrease the number of effective bubbles in the signal processing and accordingly cause the IAC measurements not reliable (Kataoka and Serizawa, 1990). Therefore, it is an important and challenging job to improve the conventional IAC measurement method with a multi-sensor probe and to enable it to be applicable in the multi-dimensional two-phase flow.

2. Interfacial measurement theorem

Since the local time-averaged IAC can be expressed by the local time-averaged value of the reciprocal interfacial velocity component in the surface normal direction in Eq. (1), we will begin the present study with the interfacial velocity investigation and further derive the relationship between the interfacial velocity and the measurable velocity of a multi-sensor probe.

When the interfaces touch a four-sensor probe, the four-sensor probe will produce two types of signals, (1) the normal interfacial signals and (2) the interfacial signals with rear sensor signal(s) ahead of the front sensor signal. The former corresponds to the oncoming interfaces touching the front sensor tip ahead of all of the rear sensor tips and the later to the receding interfaces touching at least one rear sensor tip ahead of the front sensor tip.

2.1. Derivation for an oncoming interface

Let $f_l(\mathbf{x},t)=0$ represent the lth interface. When the lth interface passes through a fixed point in space, $\mathbf{x}_0$, at time, t_{0l}, (shown by 0 in Fig. 1(a)) it satisfies

$$f_l(\mathbf{x}_0,t_{0l})=0. \tag{3}$$

Suppose that the lth interface passes through the next three adjacent fixed points in space $\mathbf{x}_1$, $\mathbf{x}_2$ and $\mathbf{x}_3$, at times, t_{1l}, t_{2l}, and t_{3l}, respectively, as shown by 1, 2 and 3 correspondingly in Fig. 1(a); that is,

$$f_l(\mathbf{x}_k,t_{kl})=0,\quad k=1,2,3. \tag{4}$$

When the point M at $\mathbf{x}_0$ in the lth interface at time t_{0l} moves to $\mathbf{x}_{M_k}$ at time, t_{kl}, $k=1$, 2, 3, it is respectively named M_k, $k=1$, 2, 3, at its corresponding time, as shown in Fig. 1(a). Thus, one has

$$f_l(\mathbf{x}_{M_k},t_{kl})=0,\quad k=1,2,3. \tag{5}$$

In the following proceeding we will encounter the distance vectors between $\mathbf{x}_0$ and $\mathbf{x}_k$, $\mathbf{s}_{0-k}$, $k=1$, 2 and 3, given by

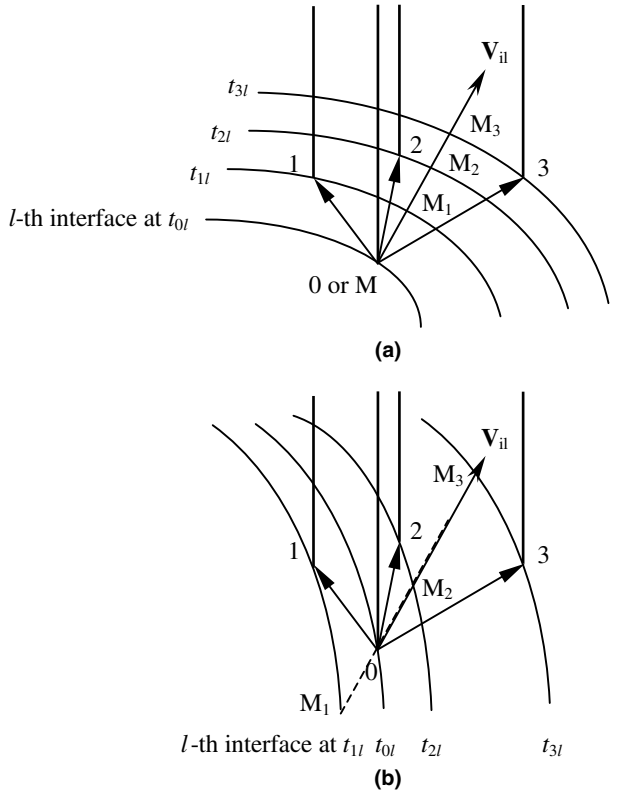

Fig. 1. Four-sensor probe and the lth interface.

$$\mathbf{s}_{0-k} = \mathbf{x}_k - \mathbf{x}_0, \quad k = 1, 2, 3, \tag{6}$$

the distance vectors between $\mathbf{x}_k$ and $\mathbf{x}_{M_k}$, $\mathbf{s}_{k-M_k}$, $k = 1$, 2 and 3, given by

$$\mathbf{s}_{k-M_k} = \mathbf{x}_{M_k} - \mathbf{x}_k, \quad k = 1, 2, 3, \tag{7}$$

and the distance vectors between $\mathbf{x}_0$ and $\mathbf{x}_{M_k}$, $\mathbf{s}_{0-M_k}$, $k = 1$, 2 and 3, given by

$$\mathbf{s}_{0-M_k} = \mathbf{x}_{M_k} - \mathbf{x}_0, \quad k = 1, 2, 3. \tag{8}$$

The three distance vectors for any k form a vector triangle and show the following relationship by combining Eqs. (6)–(8),

$$\mathbf{s}_{k-M_k} = \mathbf{s}_{0-M_k} - \mathbf{s}_{0-k}, \quad k = 1, 2, 3. \tag{9}$$

If the distances, $|\mathbf{s}_{k-M_k}|$, $k = 1$, 2, 3, is small in comparison with the length scale of the bubbly interface under consideration, the surface equations, $f_l(\mathbf{x}_k, t_{kl})$, $k = 1, 2, 3$, can be expressed by a Taylor series expansion about $\mathbf{x} = \mathbf{x}_{M_k}$ and $t = t_{kl}$, $k = 1, 2, 3$:

$$f_l(\mathbf{x}_k, t_{kl}) = f_l(\mathbf{x}_{M_k}, t_{kl}) + \nabla f_l(\mathbf{x}_{M_k}, t_{kl}) \cdot \mathbf{s}_{k-M_k} + 0 \cdot \frac{\partial f_l(\mathbf{x}_{M_k}, t_{kl})}{\partial t} + 0(\mathbf{s}_{k-M_k}), \quad k = 1, 2, 3, \tag{10}$$

where $\nabla f_l(\mathbf{x}_{M_k}, t_{kl}) \cdot \mathbf{s}_{k-M_k}$ denotes the directional derivative of $f_l(\mathbf{x}, t)$ in the direction of the distance vector, $\mathbf{s}_{k-M_k}$. Neglecting the higher-order terms in Eq. (10) and using Eqs. (4) and (5), one obtains the following relation:

$$\nabla f_l(\mathbf{x}_{M_k}, t_{kl}) \cdot \mathbf{s}_{k-M_k} = 0, \quad k = 1, 2, 3, \tag{11}$$

which implies that the surface gradient vector has a zero component in the $\mathbf{s}_{k-M_k}$ direction, i.e., the surface tangent direction.

If both the distance, $|\mathbf{s}_{0-M_k}|$, $k = 1, 2, 3$, and the time differences, $\Delta t_{0kl} = t_{kl} - t_{0l}$, $k = 1, 2, 3$, are small enough, the surface gradient vector at $(\mathbf{x}_{M_k}, t_{kl})$, $\nabla f_l(\mathbf{x}_{M_k}, t_{kl})$, $k = 1, 2, 3$, can be approximated by the surface gradient vector at $(\mathbf{x}_0, t_{0l})$, $\nabla f_l(\mathbf{x}_0, t_{0l})$, i.e.,

$$\nabla f_l(\mathbf{x}_{M_k}, t_{kl}) \approx \nabla f_l(\mathbf{x}_0, t_{0l}), \quad k = 1, 2, 3. \tag{12}$$

By inserting Eq. (9) into Eq. (11) and using Eq. (12), one gets

$$\mathbf{n}_{il} \cdot \mathbf{s}_{0-k} = \mathbf{n}_{il} \cdot \mathbf{s}_{0-M_k}, \quad k = 1, 2, 3, \tag{13}$$

where $\mathbf{n}_{il}$ is the interfacial normal unit vector of the lth interface at $(\mathbf{x}_0, t_{0l})$ and is defined by

$$\mathbf{n}_{il} = \frac{\nabla f_l(\mathbf{x}_0, t_{0l})}{|\nabla f_l(\mathbf{x}_0, t_{0l})|}. \tag{14}$$

If Eq. (13) is further divided by Δt_{0kl} $(k = 1, 2, 3)$, one gets

$$\mathbf{n}_{il} \cdot \mathbf{V}_{il} = \mathbf{n}_{il} \cdot \mathbf{V}_{m0kl} = V_{nl}, \quad k = 1, 2, 3, \tag{15}$$

where $\mathbf{V}_{il}$ is the velocity of the lth interface at $(\mathbf{x}_0, t_{0l})$, supposed to be kept constant in the interface-sensor touching process and given by

$$\mathbf{V}_{il} = \frac{\mathbf{s}_{0-M_k}}{\Delta t_{0kl}} = \frac{\mathbf{s}_{0-M_k}}{t_{kl} - t_{0l}}, \quad k = 1, 2, 3. \tag{16}$$

$\mathbf{V}_{m0kl}$ is the measurable velocities of the lth interface from sensor tip 0 to k $(k = 1, 2, 3)$ in the four-sensor probe and defined by

$$\mathbf{V}_{m0kl} = \frac{\mathbf{s}_{0-k}}{\Delta t_{0kl}} = \frac{\mathbf{s}_{0-k}}{t_{kl} - t_{0l}}, \quad k = 1, 2, 3, \tag{17}$$

and V_{nl} is the scalar product of the interfacial normal unit vector and interfacial velocity vector at $(\mathbf{x}_0, t_{0l})$ and $\mathbf{V}_{nl} = V_{nl} \cdot \mathbf{n}_{il}$ is the velocity component in the surface normal direction of the lth interface at $(\mathbf{x}_0, t_{0l})$.

Eq. (15) shows that all of the measurable interfacial velocities at a fixed position have the same velocity component in the surface normal direction and it also equals to the component of the local instantaneous interfacial velocity in the surface normal direction. It is henceforth referred to as the *Interfacial Measurement Theorem*. This theorem gives the general and important relation between the local interfacial velocity and the measurable interfacial velocities. It works not only in four-sensor probe case but also in double-sensor probe case and five-sensor probe case and so forth. The interfacial measurement theorem is the fundament for interfacial measurement with a multi-sensor probe.

2.2. Derivation for an receding interface

Because of the existence of lateral motions of an interface, it happens that some interfaces touch the rear sensor tip(s) in advance of the front sensor tip and cause the rise or fall of the output signal of the rear sensor tip(s) ahead of the front sensor tip in the four-sensor probe measurement. A conventional way to handle these receding interfaces in IAC measurement is to treat them as missing or ineffective interfaces. However, we can also derive the interfacial measurement theorem for these receding interfaces and accordingly use them effectively in the IAC evaluation for a multi-dimensional two-phase flow.

It is possible in this case that an interface will hit one, two or three rear sensor tip(s) at an earlier time than the front sensor tip. However, to clearly and simply explain the derivation, we will discuss the interface that hits one rear sensor tip ahead of the front sensor tip (0) only and take the first rear sensor tip (1) as an example. The other interface that hits any two or three rear sensor tips ahead of the front sensor tip (0) can be dealt with one by one in a similar way.

In analogy with the previous procedure in Section 2.1, one can also obtain the following equation in the lth interface at t_{1l} by the Taylor series expansion at $\mathbf{x}_{M_1}$ (see Fig. 1(b)) and know that the surface gradient vector has a zero component in the $\mathbf{s}_{1-M_1}$ direction when the interface hits the first rear sensor ahead of the front sensor only.

$$\nabla f_l(\mathbf{x}_{M_1}, t_{1l}) \cdot \mathbf{s}_{1-M_1} = 0. \tag{18}$$

If the distances, $|\mathbf{s}_{0-M_1}| = |\mathbf{x}_{M_1} - \mathbf{x}_0|$, and the time differences, $|\Delta t_{01l}| = |t_{1l} - t_{0l}|$, are also small enough, respectively, the interfacial measurement theorem in this case can be derived similarly

$$\mathbf{n}_{il} \cdot \mathbf{V}_{il} = \mathbf{n}_{il} \cdot \mathbf{V}_{m01l} = V_{nl}, \tag{19}$$

with

$$\mathbf{V}_{il} = \frac{\mathbf{s}_{0-M_1}}{\Delta t_{01l}} = \frac{\mathbf{s}_{0-M_1}}{t_{1l} - t_{0l}}, \tag{20}$$

$$\mathbf{V}_{m01l} = \frac{\mathbf{s}_{0-1}}{\Delta t_{01l}} = \frac{\mathbf{s}_{0-1}}{t_{1l} - t_{0l}}. \tag{21}$$

Eq. (19) indicates that when an interface touches the first rear sensor tip, 1, ahead of the front sensor tip, 0, the interfacial measurement theorem has the same form as in the case that the interface touches the front sensor tip, 0, ahead of the first rear sensor tip, 1. But it should be mentioned here that since $t_{1l} < t_{0l}$, the time difference in calculating the measurable velocity in this case in Eq. (21) has a negative value.

The above-mentioned discussion shows that no matter how an interface touches the four-sensor probe (in an oncoming or receding way), the interfacial velocity and the measurable interfacial velocity of the multi-sensor probe can be related by the same interfacial measurement theorem (Eq. (15)). In what follows, we shall apply the interfacial measurement theorem to the four-sensor probe measurement analysis without distinguishing between the oncoming and receding interfaces and solve it for the interfacial normal unit vector, $\mathbf{n}_{il}$, and the interfacial velocity component in the surface normal direction, $\mathbf{V}_{nl}$, which will be utilized in the derivation for the local time-averaged IAC.

3. Interfacial normal direction and interfacial velocity component in its direction

Since one can express a unit vector using the three angles between the unit vector and the three axes in a Cartesian coordinates, the local interfacial normal unit vector, $\mathbf{n}_{il}$, of the lth interface at $(\mathbf{x}_0, t_{0l})$ can be expressed by

$$\mathbf{n}_{il} = \cos\eta_{xi}\mathbf{i} + \cos\eta_{yi}\mathbf{j} + \cos\eta_{zi}\mathbf{k}, \tag{22}$$

where η_{xi}, η_{yi} and η_{zi} $(0 \leqslant \eta_{xi}, \eta_{yi}, \eta_{zi} \leqslant \pi)$ are shown in Fig. 2(a) and the 3 angles satisfy

$$\cos^2\eta_{xi} + \cos^2\eta_{yi} + \cos^2\eta_{zi} = 1. \tag{23}$$

In a four-sensor probe the three distance vectors from the front sensor tip (0) to the rear sensor tip (k), $\mathbf{s}_{0-k}$, $k = 1$, 2 and 3, are defined in Eq. (6), but are determined in fact by the geometrical configuration of the four-sensor probe. They can be expressed in a Cartesian coordinates by

$$\mathbf{s}_{0-k} = |\mathbf{s}_{0-k}|(\cos\eta_{x0k}\mathbf{i} + \cos\eta_{y0k}\mathbf{j} + \cos\eta_{z0k}\mathbf{k}), \quad k = 1, 2, 3, \tag{24}$$

where η_{x0k}, η_{y0k} and η_{z0k} $(0 \leqslant \eta_{x0k}, \eta_{y0k}, \eta_{z0k} \leqslant \pi)$, $k = 1,2,3$, are the three angles between the kth distance vectors between $\mathbf{x}_0$ and $\mathbf{x}_k$, $\mathbf{s}_{0-k}$, $(k = 1,2,3)$, and x, y and z axes, respectively, and $|\mathbf{s}_{0-k}|$ is the magnitude of $\mathbf{s}_{0-k}$. The three measurable velocities from sensor tip 0 to k, $(k = 1,2,3)$, for the lth interface, shown in Eq. (17) are accordingly expressed by

$$\mathbf{V}_{m0kl} = \frac{|\mathbf{s}_{0-k}|}{\Delta t_{0kl}}(\cos\eta_{x0k}\mathbf{i} + \cos\eta_{y0k}\mathbf{j} + \cos\eta_{z0k}\mathbf{k}), \quad k = 1, 2, 3. \tag{25}$$

The local instantaneous interfacial normal unit vector, $\mathbf{n}_{il}$, of the lth interface at $(\mathbf{x}_0, t_{0l})$, at which the front sensor tip penetrates the interface, can be solved from Eq. (15) by taking into account of Eq. (23) and the solution is shown as follows:

$$\cos\eta_{xi} = \frac{\pm|A_{01l}|}{\sqrt{A_{01l}^2 + A_{02l}^2 + A_{03l}^2}}, \tag{26}$$

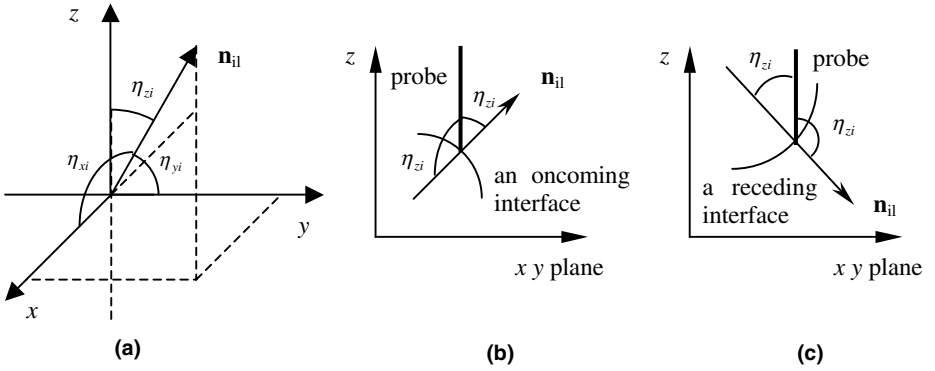

Fig. 2. Angles between $\mathbf{n}_i$ and the coordinate axes. (a) η_{xi}, η_{yi} and η_{zi}, (b) for an outcoming interface and (c) for a receding interface.

$$\cos\eta_{yi} = \frac{\pm|A_{02l}|}{\sqrt{A_{01l}^2 + A_{02l}^2 + A_{03l}^2}}, \tag{27}$$

$$\cos\eta_{zi} = \frac{\pm|A_{03l}|}{\sqrt{A_{01l}^2 + A_{02l}^2 + A_{03l}^2}}, \tag{28}$$

where A_{01l}, A_{02l} and A_{03l} are the directional determinants that are used here for the interfacial normal direction determination and are determined by the three distance vectors from the front sensor tip (0) to the rear sensor tip (k), i.e. $\mathbf{s}_{0-k}$, $k = 1, 2$ and 3, and the three time differences when the lth interface moves from the front sensor tip (0) to the rear sensor tip (k), i.e. $\Delta t_{0kl} = t_{kl} - t_{0l}$, $k = 1,2,3$. The positive Δt_{0kl} corresponds to the oncoming interface and the negative Δt_{0kl} to the receding one. These three directional determinants are given by

$$A_{01l} = \begin{vmatrix} \frac{t_{1l}-t_{0l}}{|\mathbf{s}_{0-1}|} & \cos\eta_{y01} & \cos\eta_{z01} \\ \frac{t_{2l}-t_{0l}}{|\mathbf{s}_{0-2}|} & \cos\eta_{y02} & \cos\eta_{z02} \\ \frac{t_{3l}-t_{0l}}{|\mathbf{s}_{0-3}|} & \cos\eta_{y03} & \cos\eta_{z03} \end{vmatrix}, \tag{29}$$

$$A_{02l} = \begin{vmatrix} \cos\eta_{x01} & \frac{t_{1l}-t_{0l}}{|\mathbf{s}_{0-1}|} & \cos\eta_{z01} \\ \cos\eta_{x02} & \frac{t_{2l}-t_{0l}}{|\mathbf{s}_{0-2}|} & \cos\eta_{z02} \\ \cos\eta_{x03} & \frac{t_{3l}-t_{0l}}{|\mathbf{s}_{0-3}|} & \cos\eta_{z03} \end{vmatrix}, \tag{30}$$

$$A_{03l} = \begin{vmatrix} \cos\eta_{x01} & \cos\eta_{y01} & \frac{t_{1l}-t_{0l}}{|\mathbf{s}_{0-1}|} \\ \cos\eta_{x02} & \cos\eta_{y02} & \frac{t_{2l}-t_{0l}}{|\mathbf{s}_{0-2}|} \\ \cos\eta_{x03} & \cos\eta_{y03} & \frac{t_{3l}-t_{0l}}{|\mathbf{s}_{0-3}|} \end{vmatrix}. \tag{31}$$

Since there are two surface normal directions, the outward and the inward, at any point on an interface, each of $\cos\eta_{xi}$, $\cos\eta_{yi}$ and $\cos\eta_{zi}$ in Eqs. (26)–(28) has 2 roots (positive and negative), which correspond to two complementary angles for each of η_{xi}, η_{yi} and η_{zi} in $[0, \pi]$. The positive cosine value stands for the acute angle and the negative cosine value for the obtuse angle. The two complementary angles for the oncoming and receding interfaces are shown in Fig. 2(b) and (c), respectively if η_{zi} is taken as an example. Note that the outward interfacial normal direction is usually chosen to be the positive interfacial direction and only one angle is a right solution for each interface. The positive or negative cosine value selection for each $\cos\eta_{xi}$, $\cos\eta_{yi}$ and $\cos\eta_{zi}$ in Eqs. (26)–(28) can be determined by the sign of A_{01l}, A_{02l} and A_{03l}, respectively.

The local instantaneous interface velocity component in the surface normal direction, $\mathbf{V}_{nl}$, at $(\mathbf{x}_0, t_{0l})$ can also be obtained readily by substituting $\mathbf{V}_{m0kl}$ ($k = 1,2,3$) in Eq. (25) and $\mathbf{n}_{il}$ in Eq. (22) into Eq. (15) and given by

$$\mathbf{V}_{nl} = V_{nl} \cdot \mathbf{n}_{il} = \frac{A_0}{\sqrt{A_{01l}^2 + A_{02l}^2 + A_{03l}^2}} \cdot \mathbf{n}_{il}, \tag{32}$$

where A_0 is the basic determinant of the four-sensor probe which is determined completely by the three directions of the distance vectors from the front sensor tip (0) to the rear sensor tip (k), $\mathbf{s}_{0-k}$, $k = 1$, 2 and 3, and given by

$$A_0 = \begin{vmatrix} \cos\eta_{x01} & \cos\eta_{y01} & \cos\eta_{z01} \\ \cos\eta_{x02} & \cos\eta_{y02} & \cos\eta_{z02} \\ \cos\eta_{x03} & \cos\eta_{y03} & \cos\eta_{z03} \end{vmatrix}. \tag{33}$$

4. Local time-averaged IAC

According to Kataoka et al. (1986), the local instantaneous IAC at $(\mathbf{x}_0, t_{0l})$ for the lth interface is defined as

$$a_{il}(\mathbf{x}_0, t_{0l}) = |\nabla f_l(\mathbf{x}_0, t_{0l})|\delta(f_l(\mathbf{x}_0, t_{0l})). \tag{34}$$

Upon taking the material derivative of $f_l(\mathbf{x}, t)$ at $(\mathbf{x}_0, t_{0l})$, one finds that

$$\frac{|\nabla f_l(\mathbf{x}_0, t_{0l})|}{\frac{\partial f_l(\mathbf{x}_0, t_{0l})}{\partial t}} = -\frac{1}{\mathbf{V}_{il}(\mathbf{x}_0, t_{0l}) \cdot \mathbf{n}_i(\mathbf{x}_0, t_{0l})}. \tag{35}$$

By applying the interfacial measurement theorem and substituting Eq. (35) into Eq. (34), one gets

$$a_{il}(\mathbf{x}_0, t_{0l}) = \frac{1}{|\mathbf{V}_{nl}(\mathbf{x}_0, t_{0l})|}\left|\frac{\partial f_l(\mathbf{x}_0, t_{0l})}{\partial t}\right|\delta(f_l(\mathbf{x}_0, t_{0l})). \tag{36}$$

Eq. (36) indicates the relationship between the local instantaneous IAC, a_{il}, and the local instantaneous velocity component in the surface normal direction, $\mathbf{V}_{nl}$, at $(\mathbf{x}_0, t_{0l})$ for the lth interface.

If there are many interfaces existing in the area of under consideration, the local IAC is given by

$$a_i(\mathbf{x}_0, t_{0l}) = \sum_l \frac{1}{|\mathbf{V}_{nl}(\mathbf{x}_0, t_{0l})|}\left|\frac{\partial f_l(\mathbf{x}_0, t_{0l})}{\partial t}\right|\delta(f_l(\mathbf{x}_0, t_{0l})). \tag{37}$$

Taking the time average of Eq. (37) over the time interval, Ω, the local time averaged IAC is

$$\overline{a_i}^t(\mathbf{x}_0) = \frac{1}{\Omega}\int_t^{t+\Omega} a_i(\mathbf{x}_0, t_{0l})\,\mathrm{d}t = \frac{1}{\Omega}\sum_{l=1}^{N_{ti}}\int_t^{t+\Omega}\frac{1}{|\mathbf{V}_{nl}(\mathbf{x}_0, t_{0l})|}\left|\frac{\partial f_l(\mathbf{x}_0, t_{0l})}{\partial t}\right|\delta(f_l(\mathbf{x}_0, t_{0l}))\,\mathrm{d}t, \tag{38}$$

where N_{ti} denotes the number of interfaces which pass the point, $\mathbf{x}_0$, within the time interval, Ω.

In view of Eq. (3), Eq. (38) can be rewritten as

$$\overline{a_i}^t(\mathbf{x}_0) = \frac{1}{\Omega}\sum_{l=1}^{N_{ti}}\frac{1}{|\mathbf{V}_{nl}(\mathbf{x}_0, t_{0l})|} = \frac{1}{\Omega}\sum_{l=1}^{N_{ti}}\frac{1}{|V_{nl}(\mathbf{x}_0, t_{0l})|}, \tag{39}$$

which is in accordance with the form obtained by substituting Eq. (15), i.e., interfacial measurement theorem, into Eq. (1).

Under the condition that $\mathbf{s}_{0k}$, $(k = 1, 2, 3)$, are independent of each other, which implies that the basic determinant A_0 satisfies

$$A_0 \neq 0, \tag{40}$$

the local time-averaged IAC can be derived finally by substituting Eq. (32) into Eq. (39) and is given by

$$\overline{a_i}^t(\mathbf{x}_0) = \frac{1}{\Omega}\sum_{l=1}^{N_{ti}} \frac{\sqrt{A_{01l}^2 + A_{02l}^2 + A_{03l}^2}}{|A_0|}. \tag{41}$$

With this equation, the local time-averaged IAC can be calculated within a time interval by using the geometrical parameters of the four-sensor probe and the measurable time differences when the interfaces pass through sensor tips. It is worthwhile to mention that Kataoka et al. (1986) firstly derived Eq. (41) for the oncoming interfaces in 1986 and Tan and Ishii (1990) also did the similar work for the oncoming interfaces in 1990.

5. Interface-pairing signal-processing scheme

When a probe sensor pierces or leaves a bubble, one knows that it produces a rising or falling signal. Therefore, the signal from each sensor contains basically two types of information, namely: (1) identification of phase (gas and liquid) and (2) residence time of each phase (gas and liquid). In the signal processing of a four-sensor probe measurement, there are two important selections, (1) the threshold selection in distinguishing the gas and liquid phases and (2) the right selection of four closely corresponding signals from each sensor, which is due to the fact that four sequential signals detected by the four sensors do not always correspond to the same interface, and the residence time intervals of the gas or liquid phase at the sensors are not exactly the same. We have estimated the void fraction reduction at 1.05% and the IAC reduction at 0.156% when the signal thresholds were increased 20% in the practical optical four-sensor probe measurements.

Revankar and Ishii (1992, 1993) proposed a bubble-pairing signal-processing scheme for the multi-sensor probe that was proved to be effective in one-dimensional two-phase flow measurement. Due to their assumption that the bubble moves forward and the front sensor signal rises or falls before the rear sensor signal does, the bubble-pairing signal-processing scheme has the limitation to be applied a multi-dimensional two-phase flow measurement. To meet the needs for the multi-dimensional two-phase flow measurement with the multi-sensor probe, we developed the following interface-pairing signal-processing scheme.

In this scheme, the front sensor is selected as the main sensor and other sensors are auxiliary. The measured interface is counted according to the signal of the main sensor. The auxiliary sensor signals are identified by comparison with the main sensor's signal. The signal sieving of the auxiliary sensors is made in the following way by judging if the corresponding conditions are satisfied:

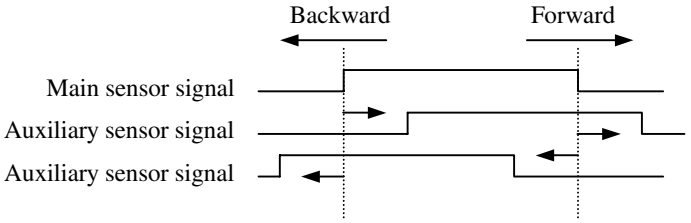

Fig. 3. Interface-pairing signal-processing scheme.

(1) The auxiliary sensor is either in the liquid phase or in the gas phase when the main sensor penetrates a head-on interface. For the case of signal rising in the main sensor, the filtration for the corresponding signal rising in the auxiliary sensors is facing forward when the auxiliary sensor is still in liquid phase and the filtration is facing backward when the auxiliary sensor is in gas phase. For the case of signal falling in the main sensor, the filtration for the corresponding signal falling in the auxiliary sensors is facing forward when the auxiliary sensor is still in gas phase and the filtration is facing backward when the auxiliary sensor is in liquid phase (see Fig. 3). All of the sensor tips penetrate into an interface within a fixed time range, namely, the three auxiliary sensor signals rise or fall closely before or after the main sensor signal does. Therefore, denoting the times of the main and the three auxiliary sensor signals by t_{0l} and t_{kl}, $k = 1$, 2 and 3, respectively, one can specify the condition by

$$|t_{0l} - t_{kl}| < \max t_k, \quad k = 1, 2, 3 \tag{42}$$

where $\max t_k$ $(k = 1, 2, 3)$ is a time constant and determined by the distance between the front sensor tip (0) and the kth rear sensor tips, $|\mathbf{s}_{0-k}|$ $(k = 1, 2, 3)$, and minimum gas velocity, $v_{g\min}$, estimated with a local drift flux model, viz.

$$\max t_i = \frac{|\mathbf{s}_{0-k}|}{v_{g\min}} = \frac{|\mathbf{s}_{0-k}|}{c \cdot v_g} = \frac{|\mathbf{s}_{0-k}|}{c \cdot (v_f + v_r)}, \quad k = 1, 2, 3, \tag{43}$$

where v_g is the estimated gas velocity, v_f is the predicted velocity distribution of liquid turbulence (Hibiki et al., 1998), v_r is the velocity difference between the two phases and, generally, takes the value of 0.1–0.3 m/s and c is a low limit constant (about 0.1).

(2) The two interfaces of a bubble either hit or miss a sensor when they pass through a sensor. There does not exist a bubble with one interface hitting a sensor and the other missing it. Thus the bubble signal outputs, $V_k(t)$, $k = 1, 2, 3$, in the auxiliary sensors should meet

$$V_k(t) > V_E, \text{ when } t_{k(2b)} \leqslant t < t_{k(2b+1)}, \quad k = 1, 2, 3 \text{ (for hitting a sensor)} \tag{44}$$

or

$$V_k(t) < V_E, \text{ when } t_{k(2b)} \leqslant t < t_{k(2b+1)}, \quad k = 1, 2, 3 \text{ (for missing a sensor)} \tag{45}$$

where V_E is the voltage threshold used to distinguish the gas phase from the liquid phase, and the subscripts, $2b$ and $2b + 1$, stand for the front and rear half surfaces of the bth bubble with regard to the main sensor (0).

(3) When the two interfaces of a bubble move toward a sensor, the front interface touches the sensor ahead of the rear interface and the signal rise happens before the signal fall for the bubble. Hence the two interfacial signals of each bubble from the same sensor should also satisfy the following condition:

$$t_{k(2b)} < t_{k(2b+1)}, \quad k = 1, 2, 3. \tag{46}$$

In the normal situation all sensors of the four-sensor probe usually penetrate into an oncoming or receding interface and output effective signals. However, because of the finite size of the probe and the lateral motions of the interfaces, it is inevitable to come across the missing interfaces which touch the main sensor and miss at least one of the auxiliary sensors and result in a flat signal output in the record of the corresponding auxiliary sensor. Moreover, due to the incompleteness of the signal-processing scheme, some interfaces touching all of the sensor tips may not meet the requirements of the signal-processing scheme in extreme cases and cannot be counted to be the effective interfaces in the signal processing. Only the signals from the effective interfaces are used in the local time-averaged IAC calculation with Eq. (41). The missing or miscounted interface is treated as if it possesses the average measured IAC of the effective interfaces.

In order to know the signal processing error due to the right selection of the same interface signal from the outputs of different sensors in the present interface-pairing signal processing scheme we compared the processed signals to the raw signals and showed that the present scheme could count almost all of the effective interfaces touching both front sensor and all rear sensors. Hence the signal processing error linked with the right selection of the same interface signal can be minimized to 0 in the present scheme.

6. Application of the improved IAC methodology

In order to validate the previous methodological improvement, an application experiment in upward air-water two-phase flow along a vertical large diameter pipe (inner diameter D: 0.2 m, the ratio of the pipe length to diameter L/D: 61.5) has been carried out using optical four-sensor probes. The schematic diagram for the experimental assembly and the probe measurements was illustrated in Fig. 4. The deviation of the electro-magnetic flow meter is within $\pm 0.1\%$ in liquid flow rate measurement and that of orifice flow meter is within $\pm 0.92\%$ in gas flow rate measurement. There were two optical four-sensor probes used at $L/D = 11.4$ and 56.7, respectively in this experiment. The shape and geometrical configuration of the optical four-sensor probes are shown in Fig. 5. The diameter of the optical fibers is 0.125 mm. The sampling frequency for each optical fiber sensor during the present data acquisition is 10 kHz. The superficial gas velocity, j_G, is estimated using the pressure at top of test section. The flow patterns are undisturbed bubbly, agitated bubbly and churn slug flows and the bubble size is greater than 3 mm within the present experimental range.

The previous analysis showed that within a time interval the local time-averaged IAC could be calculated from the three distance vectors of a four-sensor probe and the time differences when the interfaces move from the front sensor tip to the rear sensor tips by using Eq. (41) and each interface recorded in the sequential signals of the four sensors could be distinguished by using the

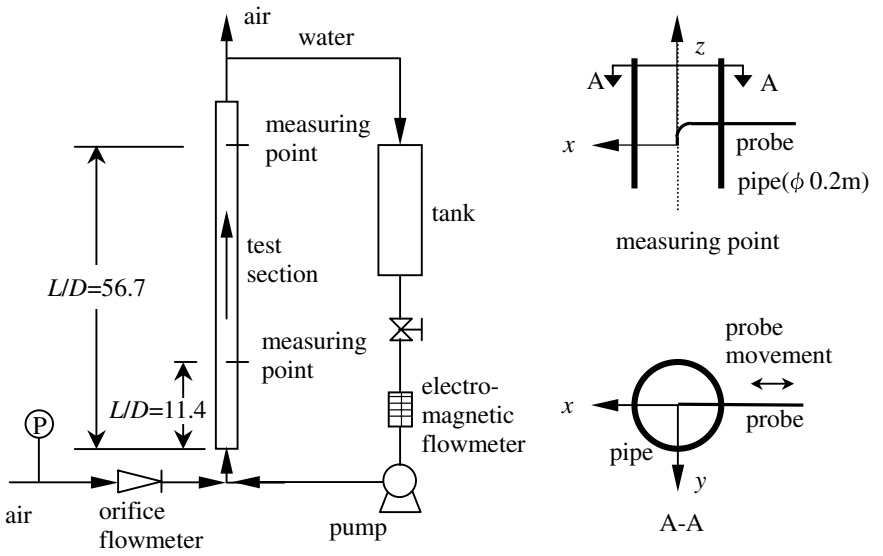

Fig. 4. The schematic diagram for the experimental assembly and the probe measurement.

newly proposed interface-pairing signal-processing scheme. Therefore, based on these methods, we measured the local time-averaged IAC with the four-sensor probes (4s) at $L/D = 11.4$ and 56.7 in the vertical large diameter pipe under various flow conditions and showed the results at $L/D = 11.4$ and 56.7 in Figs. 6 and 7, respectively by using open symbols of circle, square and triangle.

Since the local time-averaged IAC ties to the local interfacial velocity and the local bubble distribution, the experimental results in Figs. 6 and 7 have showed that it usually decreases with the increase of r/R and displays a core-peak distribution, similar to the profiles of the velocity and the gas phase. But at low j_G and undisturbed bubbly flow condition the local time-averaged IAC demonstrated a slight wall peak in its radial profile (see the symbols of circle in Fig. 6). The distribution of the local time-averaged IAC is closely linked with not only the changes of j_L and j_G but also the flow patterns in the vertical large diameter pipe. The j_G increase and the j_L decrease augment the local time-averaged IAC. The agitated bubbly and churn slug flows with the prevalence of multi-dimensional interfacial motion keep the higher local time-averaged IAC than the undisturbed bubbly flow does. The local time-averaged IAC at $L/D = 56.7$ is higher than that at $L/D = 11.4$, which can be accounted for by the flow development and the gas expansion in the vertical direction.

If the flow in the above experiments could be assumed to be one-dimensional and the double-sensor probes (2s), together with the bubble-pairing signal-processing scheme of Revankar and Ishii (1992), were applicable, we could also get the local time-averaged IAC under the same flow conditions by using two double-sensor probes and illustrated them with the solid symbols of circle, square and triangle in Figs. 6 and 7. The measured local time-averaged IAC comparison between the four-sensor probe and the double-sensor probe showed that the results from the four-sensor probe were in agreement with those from the double-sensor probe at the high j_L

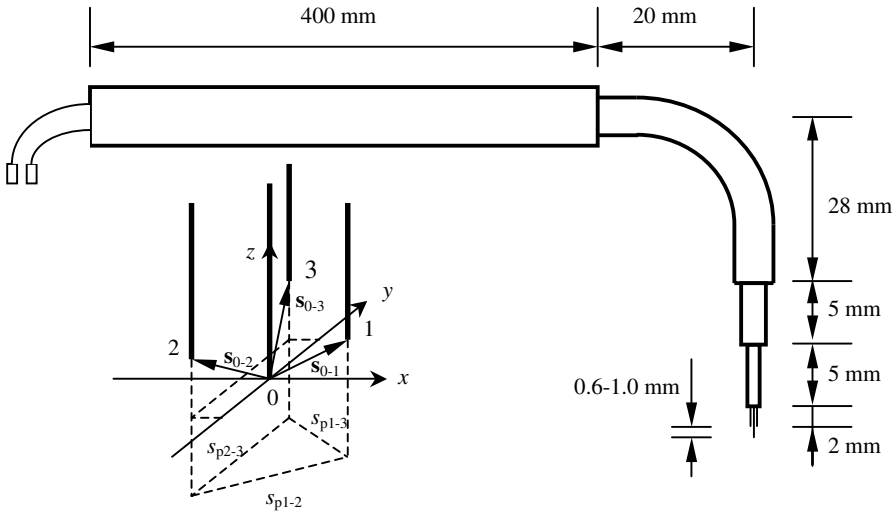

Geometrical configuration of the two optical four-sensor probes

Geometrical configuration		Probe at L/D=11.4	Probe at L/D=56.7
$\mathbf{s}_{0-1}$	$\lvert\mathbf{s}_{0-1}\rvert$	0.886 mm	0.764 mm
	η_{x01}	72.3°	70.4°
	η_{y01}	86.3°	71.6°
	η_{z01}	18.2°	27.5°
	$\lvert z_1 - z_0\rvert$	0.842 mm	0.678 mm
$\mathbf{s}_{0-2}$	$\lvert\mathbf{s}_{0-2}\rvert$	0.967 mm	0.673 mm
	η_{x02}	100°	80.3°
	η_{y02}	121°	119°
	η_{z02}	33.0°	30.8°
	$\lvert z_2 - z_0\rvert$	0.811 mm	0.578 mm
$\mathbf{s}_{0-3}$	$\lvert\mathbf{s}_{0-3}\rvert$	1.05 mm	0.611 mm
	η_{x03}	109°	126°
	η_{y03}	79.1°	83.0°
	η_{z03}	22.2°	37.3°
	$\lvert z_3 - z_0\rvert$	0.972 mm	0.486 mm
s_{p1-2}		0.709 mm	0.584 mm
s_{p1-3}		0.629 mm	0.641 mm
s_{p2-3}		0.722 mm	0.622 mm
Optical fiber diameter		0.125 mm	

Fig. 5. The shape and geometrical configuration of the optical four-sensor probes.

condition, where the bubbles usually move in an one-dimensional way, and that the double-sensor probe got a higher local time-averaged IAC value at the low j_L condition, where the multi-dimensional bubbly flow was prevailing. The difference between the four-sensor probe and the double-

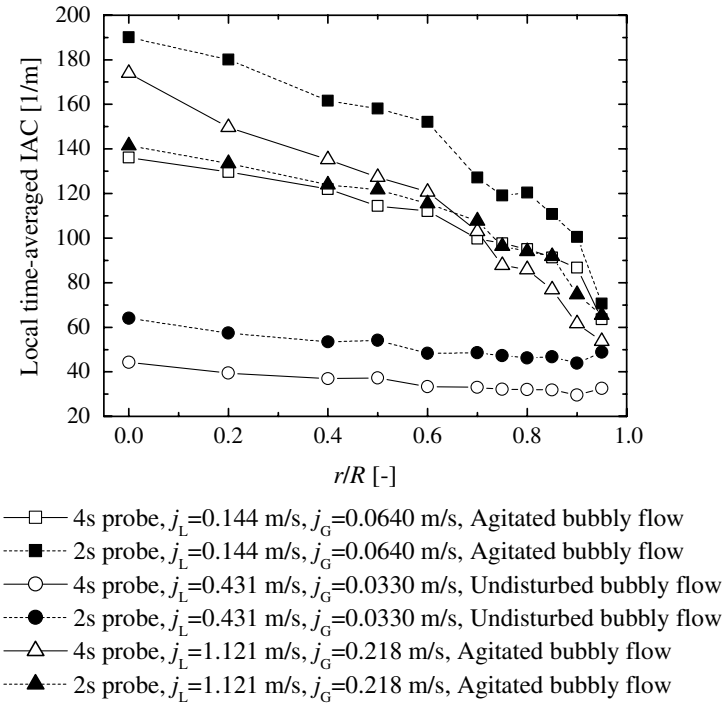

Fig. 6. Local time-averaged IAC profiles at $L/D = 11.4$.

sensor probe increases with the decrease of j_L and the decrease of r/R due to the change of the local secondary bubbly flow prevalence. The reasons for this phenomena are that the bubble shape and behavior in the multi-dimensional two-phase flow are not consistent with the required assumptions of the double-sensor probe method and the recovering way for the miscounted interfaces produced largely by the bubble-pairing scheme of Revankar and Ishii (1992) is questionable.

In the four-sensor probe measurement in a multi-dimension two-phase flow, the local time-averaged IAC contribution from each of the missing and miscounted interfaces cannot be obtained accurately and directly from the measured time information of the interface and is usually recovered indirectly by using the average measured IAC value of all effective interfaces. Wu and Ishii (1999) reported that the average IAC of the missed and miscounted interfaces at the measuring point is generally different from that of the effective interfaces. Therefore the deviation of the estimation for the missed and miscounted interfaces may not be negligible and the measured local time-averaged IAC including this estimation becomes questionable if the number of the missing and miscounted interfaces increases. In order to evaluate the reliability of the multi-sensor probe measurement, an effective interface percentage (EIP) defined by the ratio of the effective interface number and total interface number is introduced in the following analysis. The value of 1-EIP is the missing and the miscounted interface percentage.

The EIPs of the four-sensor probes (together with the present interface-pairing signal-processing scheme) in the validating experiment in a vertical large diameter pipe were obtained and illustrated with the open symbols of circle and square in Fig. 8. Since the two-phase flow at same flow

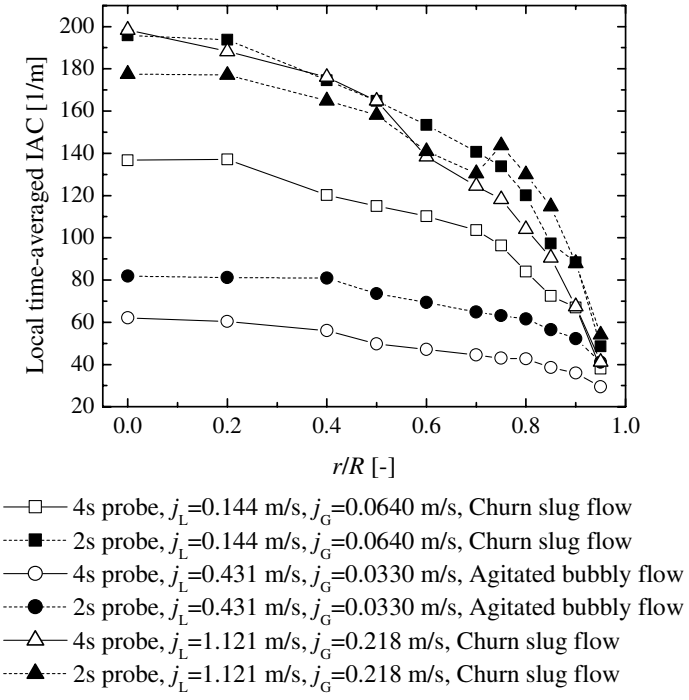

Fig. 7. Local time-averaged IAC profiles at $L/D = 56.7$.

conditions was assumed to be one-dimensional in the local time-averaged IAC measurement with the double-sensor probes, we could get the EIPs of the double-sensor probes (together with the bubble-pairing signal-processing scheme of Revankar and Ishii (1992)) and showed them with the solid symbols of circle and square in Fig. 8 too. The upper and lower parts in Fig. 8 are for the EIPs at $L/D = 56.7$ and 11.4 in the pipe, respectively. The double-sensor probe almost had the same distance separation between the front sensor tip and rear sensor tip as the four-sensor probe at the same L/D. The EIP comparison between the four-sensor probe and the double-sensor probe indicated that both of the probes had nearly equal EIP (60–70%) in one-dimensional two-phase flow (see the symbols of open and solid cycles in the lower part of Fig. 8) and that the four-sensor probe kept a high EIP (60–80%) and the double-sensor probe showed a decreasing EIP (0–50%) when the bubbly secondary flow gradually grew up. Since the multi-dimensional effect of the two-phase flow in the vertical large diameter pipe increases with the j_L decrease and the j_G increase and with the L/D increase and the r/R decrease, the EIP of the double-sensor probe decreases with the j_L decrease and the j_G increase and with the L/D increase and the r/R decrease. It was noted that the EIPs with four-sensor probes at $L/D = 56.7$ are slightly higher than those of $L/D = 11.4$ in Fig. 8. It could be accounted for by the closer distance separations between the front and rear sensor tips of the four-sensor probe at $L/D = 56.7$ than those at $L/D = 11.4$, which resulted in a lower missing interface percentage at $L/D = 56.7$ than that at $L/D = 11.4$.

Due to the sensor number increases in a four-sensor probe, its missing interface percentage is expected to be greater than that of a double-sensor probe. However, the present EIP in the four-

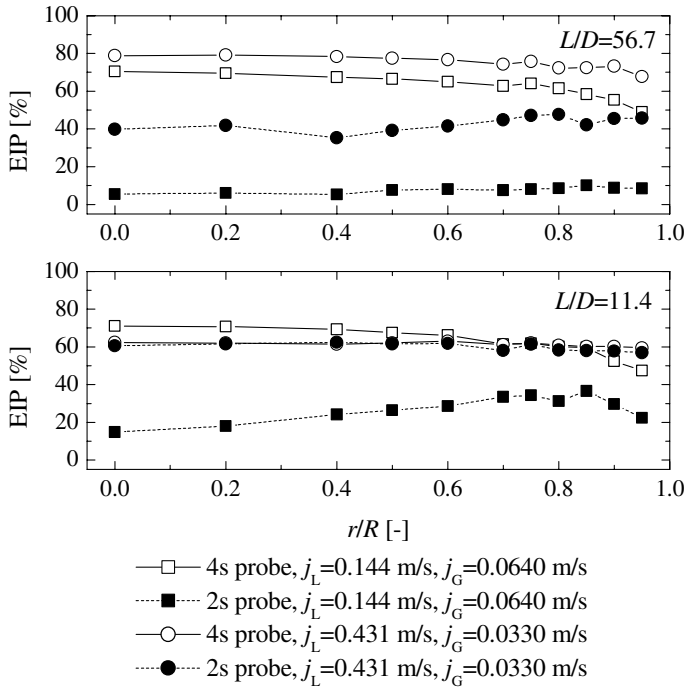

Fig. 8. Radial EIP profiles at $L/D = 11.4$ and 56.7 for the four-sensor and double-sensor probes.

sensor probe with the interface-pairing signal-processing scheme was higher than that of the double-sensor probe with the bubble-pairing signal-processing scheme when the bubbly secondary flow happened. These facts revealed that the conventional double-sensor probe method produced a large amount of miscounted interfaces and made itself unreliable in the multi-dimensional two-phase flow measurement and that the miscounted interface percentage from the present improved four-sensor probe method was negligible and the missing interface percentage increase in the four-sensor probe was not noteworthily observed by comparing with the double-sensor probe.

7. Measurement error evaluation

The intrusive probes inevitably disturb the local flow due to the finite size of the probe. The probe intrusiveness causes some bubbles to escape from the probe and some bubbles to be deformed and changed in their velocity magnitudes and directions in the probe-bubble touching processes. It is impossible for a sensor in the probe to detect the bubbles with a size same as or smaller than the sensor tip diameter in two-phase flow. The finite distance differences between the sensor tips provoke some bubbles touching one sensor tip and missing the other sensor tip(s). These effects somewhat decrease the reliability of the intrusive probe measurement and should be analyzed and evaluated carefully.

When an intrusive probe sensor penetrates a bubble, the local interface of the bubble will be deformed and a meniscus effect will happen around the sensor due to the surface tension. It will

result that the start and end time of a bubble contacting a sensor are later than the corresponding times when the bubble passes through the point at the sensor tip without the sensor in the flow. Fortunately, there exists the similarity in the interfacial meniscus effect for different sensors in the multi-sensor probe. The meniscus effects accordingly will not affect too much the measured time difference between the two different sensors for each interface. When a sensor pierces into a bubble, the bubble may slow down and deviate in the velocity direction. It is very difficult to evaluate the velocity change and the measurement error from this effect. The situation is expected to be worse for the receding bubbles than the oncoming bubbles. However, it should be noted that the counteracting force of the surface tension is very weak if the bubble has a much larger size, comparing with the sensor diameter. The bubble velocity change and the measurement error from the sensor piercing will accordingly be tiny if we only apply the probe to the two-phase flow with the bubbles having much larger size than the probe sensor diameter.

In order to investigate the escaped and missing bubbles of an intrusive probe, local quantities and the area- and volume-averaged quantities in the water pool were measured with intrusive probes and compared with each other or the results from the other measuremental method. The pool experimental apparatus is shown in Fig. 9. The pool pipe is 1.2 m in height (L) and 50 mm in inner diameter (D). The air flows into the pipe through an injector with 0.5 mm in inner diameter. The inlet air flow rate and pressure were measured with the rotameter and manometer, respectively. The measurement errors of the rotameter and manometer are within $\pm 0.5\%$ and $\pm 0.3\%$, respectively. The probe measuring points, A, B and C, are located at the heights of $L/D = 3.33$, 10.0 and 16.7, respectively.

If we use A ($A = \int_0^R 2\pi r \, dr$) to stand for the pipe cross-sectional area and H_0 and H_1 for the water heights in the pool without and with air passing through respectively, the volume-averaged void fraction in the pool can be expressed by

$$\bar{\alpha}^V = \frac{(H_1 - H_0) \cdot A}{H_1 \cdot A} = \frac{H_1 - H_0}{H_1}. \tag{47}$$

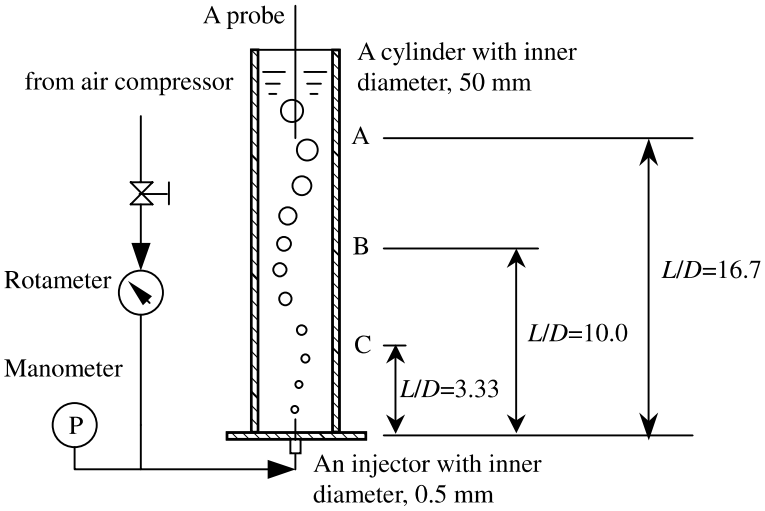

Fig. 9. Pool experimental apparatus.

We shall henceforth refer to this volume-averaged void fraction measurement as the water level measurement.

Since we usually ignore the parameter change in the circumferential direction in a vertical cylindrical pipe, the three-dimensional local time-averaged void fraction $\alpha(r,\theta,z)$ can be simplified by two-dimensional one, $\alpha(r,z)$, namely

$$\alpha(r,z) = \frac{\int_0^{2\pi} \alpha(r,\theta,z)\,\mathrm{d}\theta}{2\pi} \approx \alpha(r,\theta,z). \tag{48}$$

The two-dimensional local time-averaged void fraction $\alpha(r,z)$ is the measured quantity of the intrusive probe in this pool experiment. Thus we can express the area-averaged $\alpha(r,z)$ at any height, z, in the flow path and the volume-averaged time-averaged $\alpha\ (r,z)$, respectively by

$$\bar{\alpha}^A(z) = \frac{\int_0^R 2\pi r\alpha(r,z)\,\mathrm{d}r}{A} \tag{49}$$

and

$$\bar{\alpha}^V = \frac{\int_0^{H_1}\int_0^R 2\pi r\alpha(r,z)\,\mathrm{d}r\,\mathrm{d}z}{H_1 A}. \tag{50}$$

Comparing with Eq. (47), we knew from Eq. (50) that the $\bar{\alpha}^V$ could also be obtained from the probe measurement. To distinguish them in the follow analysis, we referred to the two $\bar{\alpha}^V$ from the water level and probe measurements as $\bar{\alpha}_L^V$ and $\bar{\alpha}_P^V$, respectively. The measured $\bar{\alpha}_L^V$ and $\bar{\alpha}_P^V$ in the upward-moving bubbly flow in a pool were shown in the upper part of Fig. 10. The comparison indicated that the $\bar{\alpha}_L^V$ is always higher than the $\bar{\alpha}_P^V$ and the difference slightly decreases with the increasing j_G. Since the water level measurement is a very reliable method for the volume-averaged void fraction measurement, the volume-averaged void fraction difference between the water level

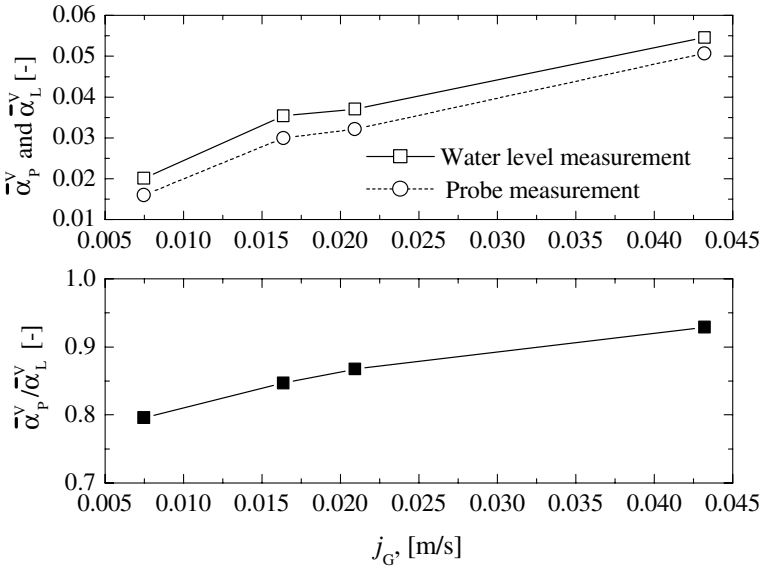

Fig. 10. Volume-averaged void fraction comparison between water level and probe measurements.

and probe measurement stands for the undetectable void fraction contributed by the escaped bubbles due to the existence of the intrusive probe. The change of $\bar{\alpha}_P^V/\bar{\alpha}_L^V$ with the j_G was shown in the low part of Fig. 10. It showed that about 79–92% (averaging 85%) of the upward-moving gas phase in the pool could be sensed by a probe and the rest part (averaging 15%) escaped from the probe touching due to the probe intrusiveness. The $\bar{\alpha}_P^V/\bar{\alpha}_L^V$ significantly increased with the increasing j_G, which revealed that the escaped bubbles decrease considerably with the increase of j_G in the upward-moving two-phase flow in a pool.

In the measurement of local time-averaged IAC only the signals from the bubbles touching both the front and rear sensors can be handled effectively. In order to investigate the probabilities of the effective and missing bubbles quantitatively, the void fractions in the upward-moving two-phase flow in a pool were measured with a double-sensor probe (0.8 mm in sensor tip separation) arranged in downward and upward facing ways. The $\bar{\alpha}^A_{\text{down\_0}}$ and $\bar{\alpha}^A_{\text{down\_1}}$ signify the cross-sectional area-averaged void fractions measured with the front (0) and rear (1) sensors of the downward (down) facing double-sensor probe, respectively and the $\bar{\alpha}^A_{\text{up\_0}}$ and $\bar{\alpha}^A_{\text{up\_1}}$ stand for those from the front (0) and rear (1) sensors of the upward (up) facing double-sensor probe. Their measured values were shown in the upper part of Fig. 11. We also compared these values by using their relative values, $\frac{\bar{\alpha}^A_{\text{down\_0}}}{\bar{\alpha}^A_{\text{down\_0}}}$, $\frac{\bar{\alpha}^A_{\text{down\_1}}}{\bar{\alpha}^A_{\text{down\_0}}}$, $\frac{\bar{\alpha}^A_{up\_0}}{\bar{\alpha}^A_{\text{down\_0}}}$ and $\frac{\bar{\alpha}^A_{up\_1}}{\bar{\alpha}^A_{\text{down\_0}}}$, and illustrated these relative values with the symbols of open square, solid square, open circle and solid circle, respectively in the lower part of Fig. 11. These relative cross-sectional area-averaged void fractions were the actual detectable bubbly percentages relative to the front sensor of the downward double-sensor probe. The comparisons indicated that the upward facing probe (represented by the front sensor) detects about 70% of bubbles

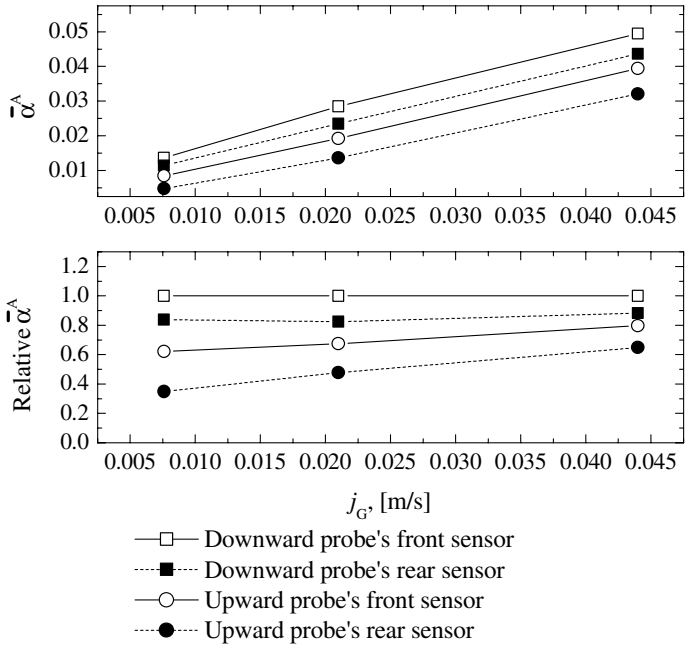

Fig. 11. Area-averaged void fraction comparison of the front and rear sensors of the downward and upward double-sensor probes.

in the pool. One can know directly that about 30% (=1–70%) of the upward-moving bubbles escape from the touching of the upward facing probe in the pool due to the existence of the rear part of the probe sensors. Thus, it can be approximately inferred that about 30% of the downward-moving bubbles will escape from the touching of the downward facing probe in the pool due to the existence of the rear part of the probe sensors. The $\frac{\bar{\alpha}^A_{\text{up\_0}}}{\bar{\alpha}^A_{\text{down\_0}}}$ in the lower part of Fig. 11 increased significantly with the increasing j_G. So one could predict presumably that the ratio of the escaped bubbles among the downward-moving bubbles might decrease significantly with the increasing j_G in the downward facing probe measurement.

The relative cross-sectional area-averaged void fractions in the lower part of Fig. 11 also showed that the rear sensor tips of the downward and upward facing probes detected about 85% and 50% of upward-moving bubbles, respectively. Thus one could know that about 15% (=1–85%) of the upward-moving bubbles touched the front sensor tip and missed the rear one in the downward facing probe measurement in the pool due to the probe sensor tip separation. The $\frac{\bar{\alpha}^A_{\text{down\_1}}}{\bar{\alpha}^A_{\text{down\_0}}}$ in the lower part of Fig. 11 increased gradually with the increasing j_G. So one could also know that the missing bubble ratio decreased gradually with the increasing j_G in the multi-sensor probe measurement.

In order to knew the ingredients of the bubbles in a multi-dimensional two-phase flow, we defined N_t as the number of bubbles detected by the front sensor of the downward facing double-sensor probe, N_{downward} as the number of bubbles moving downwardly and touching the rear sensor tip ahead of the front sensor tip, N_{upward} as the number of bubbles moving upwardly and touching the front sensor tip ahead of the rear sensor tip, and N_{missing} as the number of bubbles touching the front sensor tip but missing the rear sensor tip. The ratios of N_{downward}/N_t, N_{upward}/N_t and N_{missing}/N_t then stood for the downward bubbly rate, upward bubbly rate and missing bubbly rate, respectively. Under various j_G flow conditions in the ϕ 50 mm pipe pool, the radial profiles of the above ratios were shown in Fig. 12. The figure revealed that less than 10% (averaging 5%) of the bubbles moved downwardly and the downward-moving bubble rate increased with the increasing j_G and decreased in the radial direction. Nearly 80% of the bubbles moved upwardly in the pool and the N_{upward}/N_t also decreased in the radial direction. Over 10% (averaging 15%) were the missing bubbles and the missing bubbly rate decreased with the increasing j_G and the decreasing radius.

Based on the previous discussions, we performed a comprehensive measurement error evaluation for the downward facing double-sensor probe used in the upward-moving two-phase flow in a pool and illustrated the analysis in details in Fig. 13. The evaluation showed that about 72.14% of the bubbles touch both sensor tips and that the total escaped bubble and missing bubble rates are nearly 15.75% and 12.11%, respectively. If the present interface-pairing signal-processing scheme is used, the miscounted bubbles will be negligible and all of the bubbles touching both sensor tips will be effective. Thus the effective bubble rate will reach 72.14%. In the total IAC measurement with double- and four-sensor probes, we usually compensate for the missing bubbles by using the average effective bubbles. Since the missing bubble rate (12.11%) is not high, the compensation error for the missing bubbles may be neglected. Therefore, taking into account of the nearly even bubble size distribution (3–5 mm in bubble size) in the present two-phase flow, we can estimate the total error in void fraction and IAC measurement with the intrusive probe at about 15.75% in the

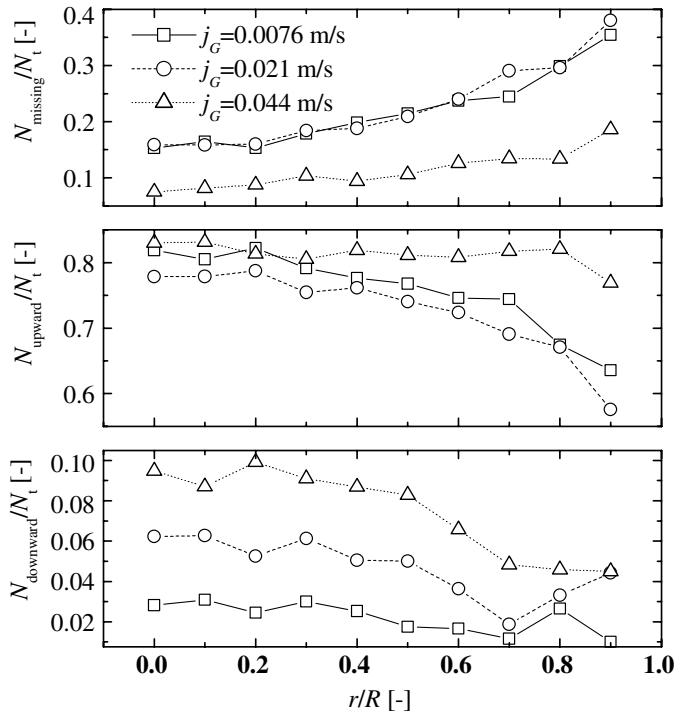

Fig. 12. The radial profiles of N_{downward}/N_t, N_{upward}/N_t and N_{missing}/N_t.

pool due to the escaped bubbles. The previous analyses also indicated that the escaped and missing bubbles decrease significantly with the bubble velocity increase. Therefore, it can be predicted that the measurement error decreases considerably in the two-phase flow in a pipe with net liquid flow and higher gas velocity.

8. Summary and conclusion

This paper presented a way for the multi-dimensional two-phase flow measurement by improving the conventional intrusive four-sensor probe methodology. In the methodological improvement and the succedent practical application and measurement error evaluation, the following conclusions can be presented.

(1) There exists an interfacial measurement theorem in the multi-sensor probe measurement. The theorem gives the general relation between the local instantaneous interfacial velocity and the measurable velocity of the multi-sensor probe. It is valid not only for the oncoming interfaces but also for the receding interfaces.
(2) With the application of the interfacial measurement theorem, the local instantaneous formulations for the interfacial normal direction and interfacial velocity component in the direction have been derived and the local time-averaged formulation of the IAC has been obtained theoretically.

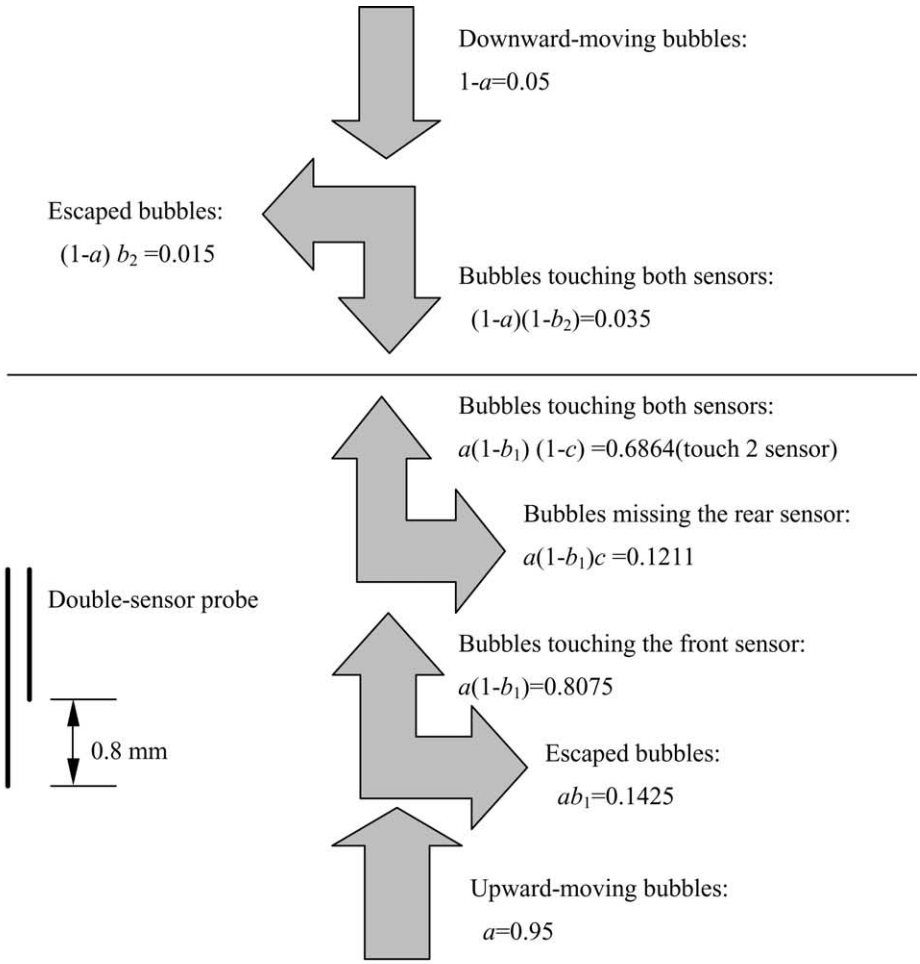

a: Upward-moving bubble rate (including the missing bubbles), (=0.8+0.15=0.95)

b_1: Escaped bubble rate for the upward-moving bubbles, (=0.15)

b_2: Escaped bubble rate for the downward-moving bubbles, (=0.3)

c: Missing bubble rate for the upward-moving bubbles, (=0.15)

Rate of the bubbles touching both sensors: $a(1-b_1)(1-c)+ (1-a) (1-b_2)=0.7214$

Total escaped bubble rate: $ab_1+(1-a)\, b_2 =0.1575$

Total missing bubble rate: $a(1-b_1)c ==0.1211$

Fig. 13. Measurement error evaluation in the two-phase flow in a pool.

(3) A new interface-pairing signal-processing scheme has been proposed to identify the effective interfaces from all oncoming and receding interfaces. Its practical application proved it to be highly effective. With the help of the interfacial measurement theorem and the new scheme,

almost all of the interfaces touching all sensors can be effectively utilized and the miscounted interface percentage is negligible in the four-sensor probe measurements.

(4) The application of the improved IAC methodology to the two-phase flow in a vertical large diameter pipe has showed that the four-sensor probes (together with the interface-pairing signal-processing scheme) can effectively measure the local time-averaged IACs with high effective interface percentages not only in the one-dimensional two-phase flow but also in the multi-dimensional two-phase flow.

(5) The measurement errors from the sensor piercing into a bubble were analyzed and it showed that the measurement error from the bubble deformation was negligible in measuring the interfacial passing time from one sensor to the others and that the measurement error from the bubble velocity variation was tiny if we only applied the probe to the two-phase flow with the bubbles having much larger size than the probe sensor diameter. The measurement errors from the escaped and missing bubbles were evaluated by performing an experiment in a pooling two-phase flow. The evaluation showed that the measurement errors from the escaped and missing bubbles were about 15.75% and nearly 0%, respectively in the two-phase flow in a pool. As a result of that, the total measurement error from these effects was estimated at about 15.75% in the two-phase flow in a pool due to the intrusiveness of the multi-sensor probe. Since the escaped and missing bubbles will decrease significantly in the two-phase flow in a pipe with net liquid flow and higher gas velocities, the total measurement errors are expected to further decrease in the circumstances.

Acknowledgments

The authors would like to acknowledge Dr. Takashi Hibiki (Research Reactor Institute, Kyoto University, Japan) for his valuable discussions and Mr. Yoshitaka Inoue (Kobe Steel, limited, Japan) for his invaluable helps. A part of this work was performed under the auspices of JAERI (Japan Atomic Energy Research Institute) and COE (Center of Excellence, Japan).

References

Delhaye, J.M., Bricard, P., 1994. Interfacial area in bubbly flow: experimental data and correlations. J. Nucl. Engng. Des. 151, 65–77.

Euh, D.J., Yun, B.J., Song, C.H., Kwon, T.S., Chung, M.K., Lee, U.C., 2001. Development of the five-sensor conductivity probe method for the local interfacial area concentration. J. Nucl. Engng. Des. 205, 35–51.

Hibiki, T., Hogsett, T., Ishii, M., 1998. Local measurement of interfacial area, interfacial velocity and turbulence in two-phase flow. J. Nucl. Engng. Des. 184, 287–304.

Ishii, M., 1975. Thermo-fluid Dynamic Theory of Two-phase Flow. Eyrolles Paris. Pp99, 145ff.

Kataoka, I., Ishii, M., Serizawa, A., 1986. Local formulation and measurements of interfacial area concentration in two-phase flow. Int. J. Multiphase Flow 12, 505–529.

Kataoka, I., Serizawa, A., 1990. Interfacial area concentration in bubble flow. J. Nucl. Engng. Des. 120, 163–180.

Kim, S., Fu, X.Y., Wang, X., Ishii, M., 2001. Study on interfacial structures in slug flows using a miniaturized four-sensor conductivity probe. J. Nucl. Engng. Des. 204, 45–55.

Revankar, S.T., Ishii, M., 1993. Theory and measurement of local interfacial area using a four sensor probe in two-phase flow. Int. J. Heat Mass Transfer 36, 2997–3007.

Revankar, S.T., Ishii, M., 1992. Local interfacial area measurement in bubble flow. Int. J. Heat Mass Transfer 35, 913–925.

Tan, M.J., Ishii, M., 1990. A method for measurement of local specific interfacial area. Int. J. Multiphase Flow 16, 353–358.

Wu, Q., Ishii, M., 1999. Sensitivity study on double-sensor conductivity probe for the measurement of interfacial area concentration in bubble flow. Int. J. Multiphase Flow 25, 155–173.